GSA Data Repository 2018164

Supercritical river terraces generated by hydraulic and geomorphic interactions—Supplementary Information

Edwin R.C. Baynes*, Dimitri Lague, Jean-Jacques Kermarrec

Univ Rennes, CNRS, Géosciences Rennes - UMR 6118, 35000 Rennes, France

*Email address: edwin.baynes@univ-rennes1.fr

Section 1: Relevance of experiments for natural channels and experimental setup.

Experimental modelling studies of landscape and fluvial dynamics are typically performed using one of two approaches. The first directly scales the experimental prototype to the natural system by ensuring that non-dimensional hydraulic parameters such as the Froude number are scaled strictly and the physical processes (e.g., sediment transport) are the same in both the experimental and natural systems. The second approach relaxes this strict scaling, and seeks a 'similarity of process' between the experiment and the natural channel (Hooke, 1968) whereby the behaviour of the processes within the experiment system are qualitatively similar and 'reasonably effective' at replicating the behaviour of natural systems despite large differences in the governing dimensionless numbers (Paola et al., 2009). This second approach has the benefit of allowing temporal and spatial timescales to be relaxed, as materials such as silica cement that is eroded by clear water flow can be used to replicate bedrock, and experiments exploring bedrock erosion processes can be performed relatively quickly. It should be noted that the results from these experiments cannot be directly scaled up to any particular natural system. Additionally, the experimental channel is always 'active', and the experiments do not include the periods of time between flood events when the channel is not being eroded, creating a difficulty when exploring relative timescales of geomorphic response between the experiments and natural rivers. However, processes such as flow acceleration above the knickpoint lip, cyclic step development, plunge pool erosion, undercutting of the knickpoint face and channel banks, cantilever failure, erosion and transport of cohesive material by hydraulic shear are present in the experiments. The typical width-depth ratio of the experimental channels at the start of the experiments (alluvial channel conditions) is 50-80, similar to that of natural gravel-bedded rivers (Finnegan et al., 2005), and the scaling of the channel width with discharge observed in natural rivers is also reproduced in the experiment. Therefore, we can be confident that the experiments are 'reasonably effective' in replicating natural processes, and the response of the channels to the perturbations (sediment supply, discharge or slope) in the experiments can help inform the response of natural channels to similar forcing.

Figure DR1 shows the setup used during our experiments in the Bedrock River Experimental Incision Tank at the Université de Rennes. The initial alluvial cover was composed of well-sorted sand (grain size = 250 μm), and the homogenous cohesive silica paste used as a bedrock simulant was composed of 61.5% angular silica, 20.5% spherical beads and 18% water. The silica paste was mixed in a cement mixer before being transferred into the box flume and homogenised using a high frequency vibrating needle to re-liquefy the paste (see Baynes et al., 2018 for further details related to the properties of the silica paste and the preparation procedure). Flow in the channel is typically laminar with low Reynolds

numbers (< 1000), and is input into the channel through a reservoir and the discharge magnitude controlled using a pump.

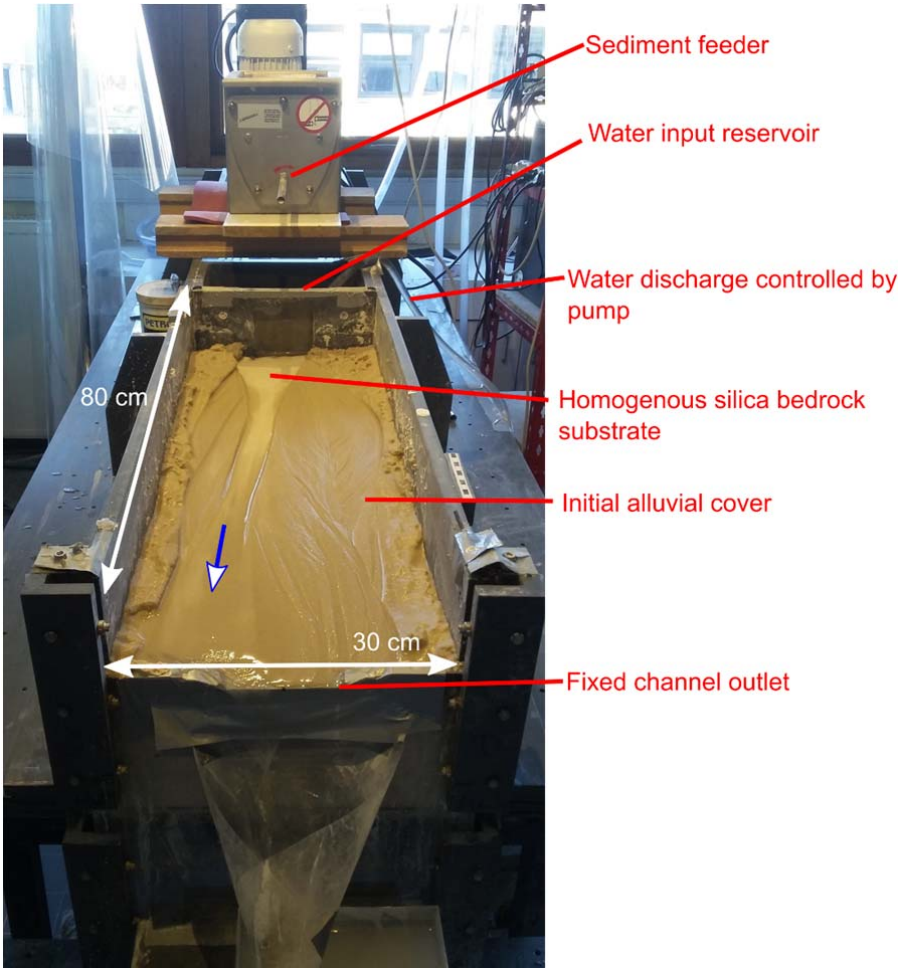

Fig. DR1: Photograph of the Bedrock River Experimental Incision Tank at Université de Rennes. The blue arrow shows the flow direction within the channel.

Section 2: *Floodos* parameters

Floodos is a numerical precipiton-based hydrodynamic model (see Davy et al., 2017 for full technical description of the model), and was used here to assess the hydraulic conditions during the experiments. The input topography for *Floodos* was produced directly by gridding the point clouds, collected from the terrestrial laser scanner at regular time intervals during the experiments, with a pixel size of 2 mm. *Floodos* was run using the laminar flow option consistent with the relatively low Reynolds number of the experiment (< 1000) across most of the channel under alluvial conditions (Fig. DR2).

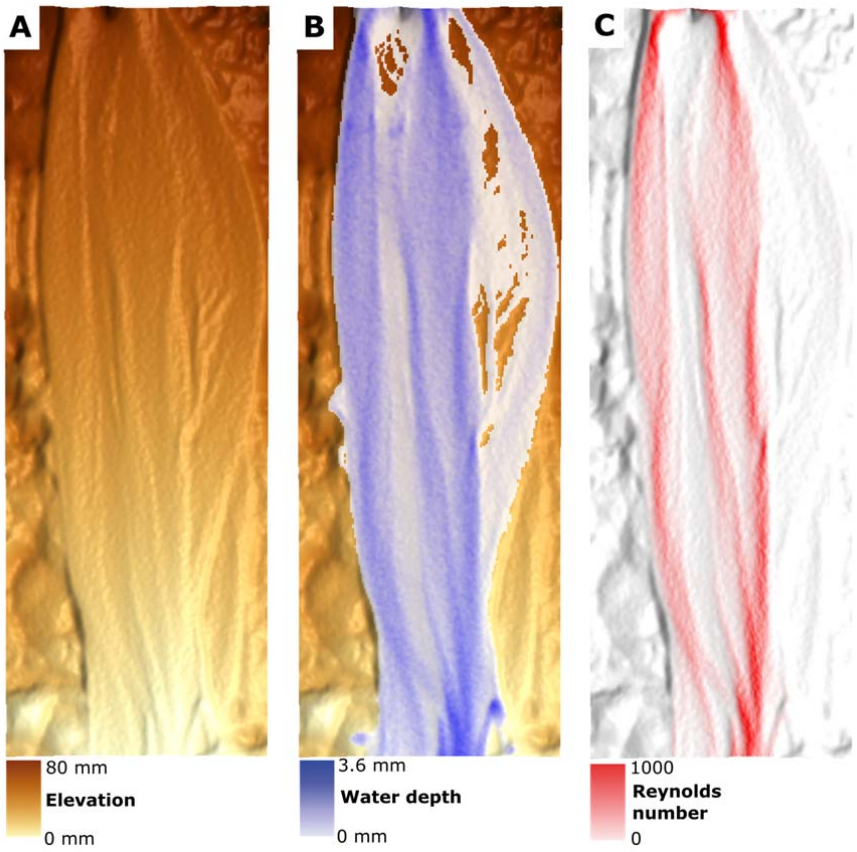

Fig. DR2: (A) Digital Elevation Model from Experiment 1, when the channel is under fully alluvial conditions (t = 33 minutes). (B) Modelled water depth mask using *Floodos* hydrodynamic model (Davy et al., 2017). (C) Calculated Reynolds number for each pixel of the flow, using the *Floodos* model output.

Under the laminar flow conditions, the local vertically averaged velocity U is approximated by:

$$U = CH^2S, \qquad \text{(S1)}$$

where C if a friction coefficient in $[L^{-1}.T^{-1}]$, H is local water depth and S is the local channel slope. Equation S1 is obtained by integrating vertically a laminar flow velocity profile assuming steady-uniform flow. In pure laminar flow, C is entirely set by the water viscosity μ and should be approximately $C \sim \rho g/3\mu$ where ρ is water density and g is gravitational acceleration. This predicts that at 10°c, C ~ 2.5 x 10^6 $m^{-1}.s^{-1}$. Fig. S2 shows the impact of different values of C on the predicted extent of water flowing over a flat surface compared to manual measurements of the wetted area obtained from a photograph taken from above the experiment (Fig. DR3A). The simulations of flow extent are relatively similar for all modelled values of C, although lower values of C predict a greater level of overflow on the edges in the downstream part. We therefore used the value of C (2.5 x 10^6 $m^{-1}.s^{-1}$) for the simulations presented here, due to good consistency with the manual measurements and the theoretical prediction of the friction coefficient based on the water viscosity for flow over a flat surface (Fig. DR 3) and for channelised flow (Fig. DR4).

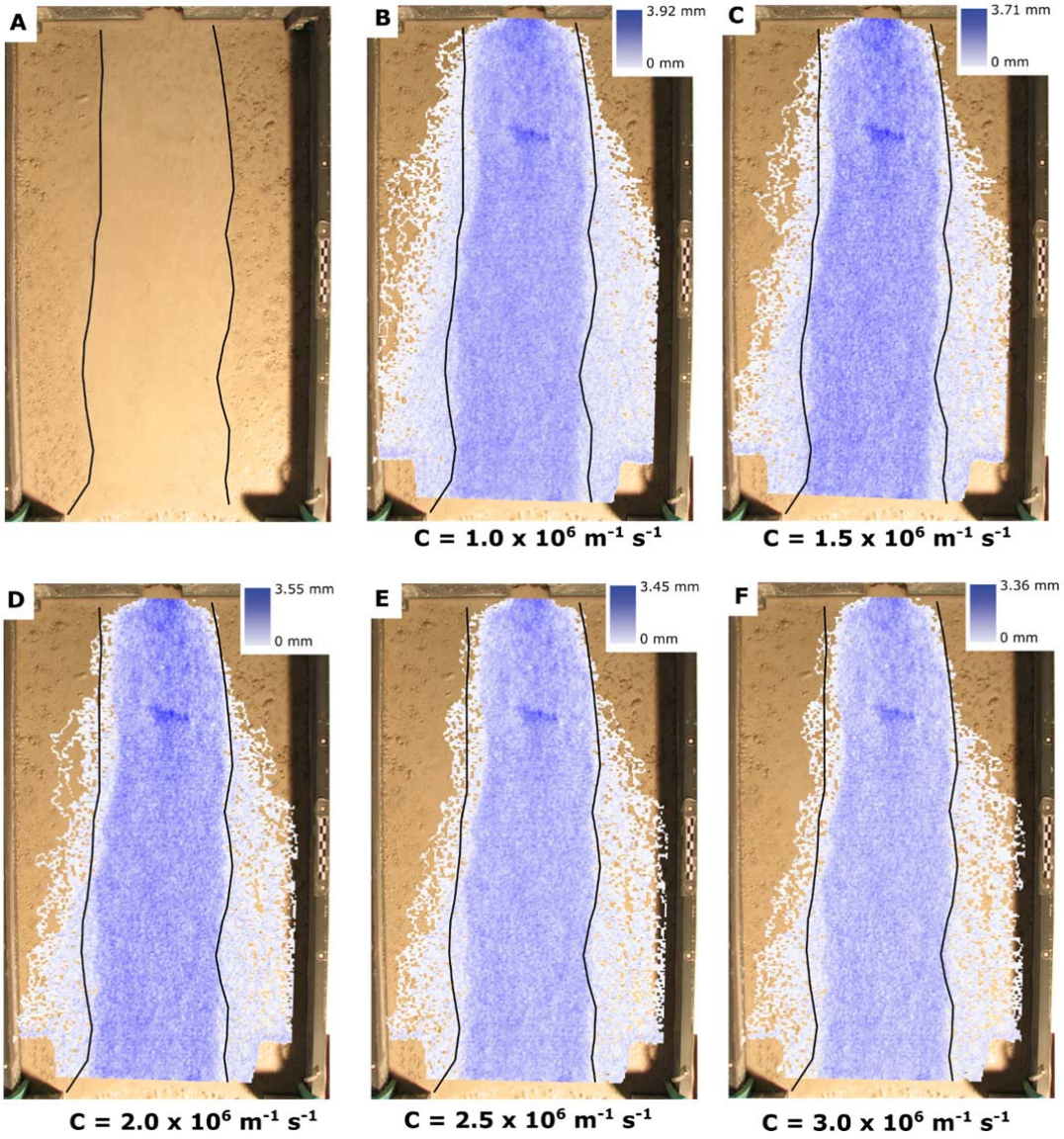

Fig. DR3: (A) Photograph of water flowing over a flat surface (slope = 3.3°, Q = 1 l/min), with black lines indicating edge of water extent measured manually from the image. Flow is from top to bottom in the image. (B-F) *Floodos* hydrodynamic model output using laminar flow option and different values of the friction coefficient. Black lines are the same as (A) and shown for comparison of modelled against observed flow extent. The predicted theoretical value of the friction coefficient (2.5 x 10^6 m^{-1} s^{-1}) has a good match with the observed flow extent. For this value, the lateral areas where overflow occurs have flow depth that are extremely low (< 0.1 mm) and represent a negligible fraction of the total discharge.

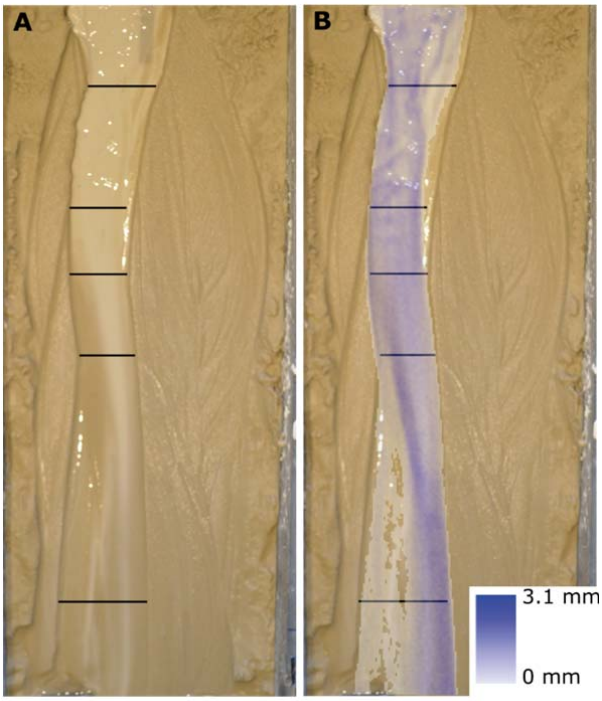

Fig. DR4: (A) Photograph of experiment 1 (t = 66 mins), with wetted area indicated by the black bars. Flow is from top to bottom in the image. (B) Floodos model water mask coloured by water depth, using friction coefficient of 2.5 x 10^6 m^{-1} s^{-1}, for the same time period overlain over the photograph, with the same black bars from (A). The Floodos water mask closely matches the manual measurements of channel width from the photograph throughout the length of the channel. At the left hand side in the downstream reach, a terrace is starting to be abandoned, hence the very low flow depths in this region.

Section 3: Evolution of channel and terrace geometry during experiments

This SI section provides the complete experimental data for the evolution of the channel geometry for each of the three experiments. The long profiles were extracted by finding the point of minimum elevation for each row of the grid (Fig. DR5). Terraces were defined from the DEM as flat surfaces (elevation within 1mm) and at least 2 cm wide. The channel cross-sections (Fig. DR6) were extracted from the data at the location of the grid that was 25% of the distance from the inlet to the outlet of the channel.

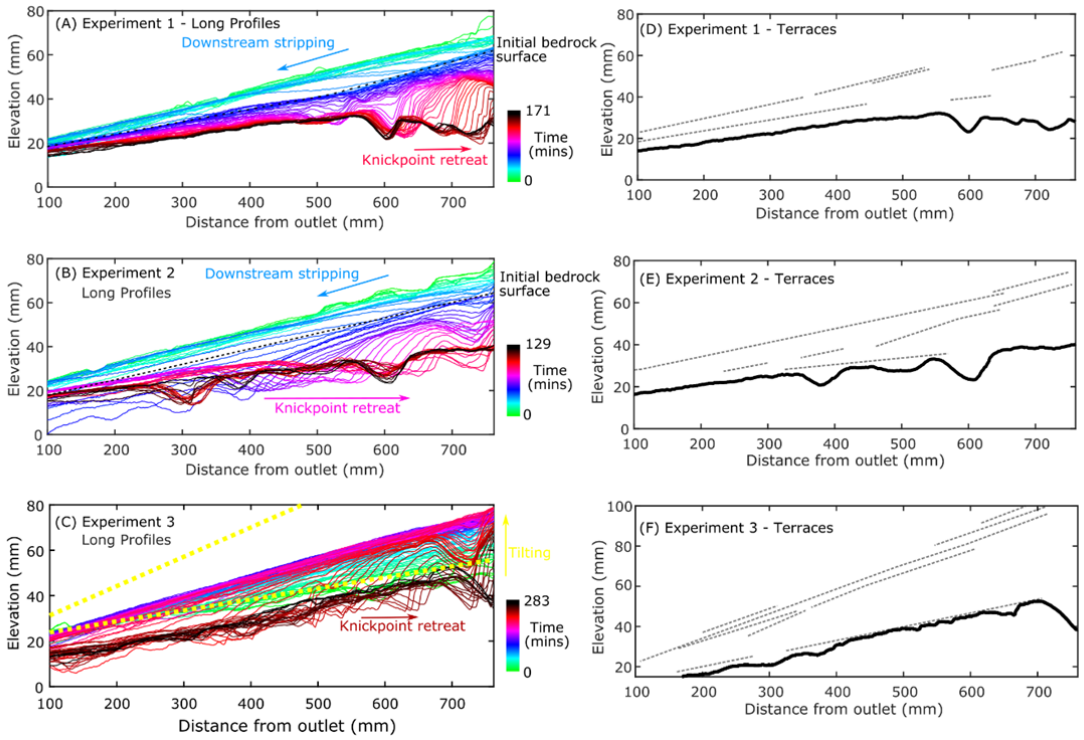

Fig. DR5: (A-C) Extracted long profiles from the three experiments. (A) Experiment 1, where the input sediment flux was stopped after 37 minutes (80 profiles in total). (B) Experiment 2, where the discharge was doubled to 3 l/min after 37 minutes (61 profiles in total). (C) Experiment 3, where the slope was increased at 1° per 60 minutes from an initial slope of 2° for 280 minutes (132 profiles in total). The colour of the lines indicates the evolution during the experiments. The dashed yellow lines in (C) show the initial slope of the experiment (2.5°), and the projected slope of the channel at the end of the tilting if there had been no erosion of the alluvial cover or bedrock (7.2°). The maximum slope achieved in the channel before the onset of the incision of bedrock was ~4.5°. Grey dashed lines in (A) and (B) indicate the elevation of the bedrock surface at the start of each experiment, to show the transition from alluvial stripping and bedrock incision. The same line is not shown in (C) as the elevation of the bedrock surface changed during the course of the experiment due to the tilting. (D-F) Preserved terrace surfaces at the end of each experiment. Solid lines indicate the long profile of the active channel, and dashed lines indicate the location and elevation of terraces. The slope of the upper terraces is greater than the incised active channel.

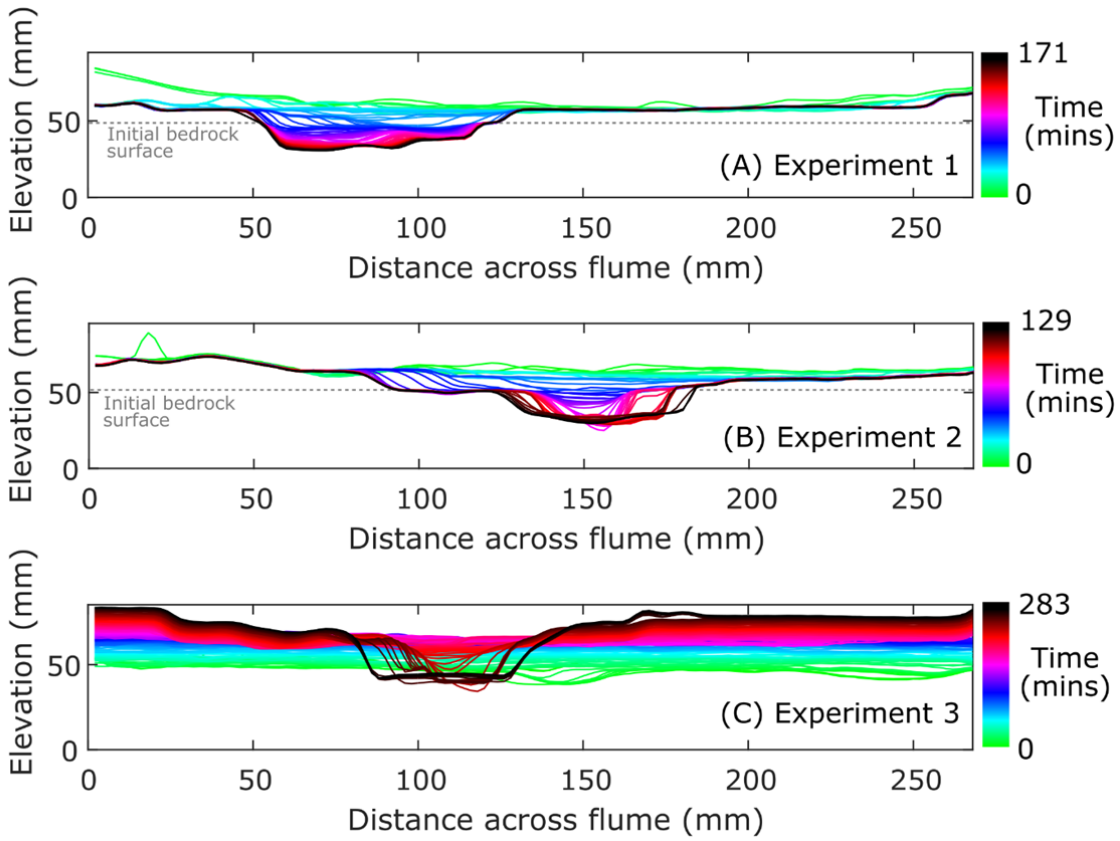

Fig. DR6: Evolution of channel cross-sections at the 25% position from the water inlet. Cross-sections were extracted from this location to ensure it was located over an area that experienced incision and the development and propagation of a knickpoint. Colours represent the same time points as Fig. S1. It can be seen that channel incision occurred under narrow channel width conditions, followed by lateral erosion of the banks leading to channel widening and minor channel aggradation in experiments 2 and 3. Grey dashed lines in (A) and (B) indicate the elevation of the bedrock surface at the start of each experiment, to show the transition from alluvial stripping and bedrock incision. The same line is not shown in (C) as the elevation of the bedrock surface changed during the course of the experiment due to the tilting.

Section 4: Demonstration of the incisional efficiency of the headward erosion process and width-incision coupling

Here, we provide further analysis to demonstrate the bedrock erosional efficiency of the headward migration of knickpoints compared to the vertical erosion by hydraulic shear upstream of the knickpoint lip (Fig. DR7). Fig. DR7A shows selected long profiles from experiment 1 and Fig. DR8B shows the rate of elevation change along the profiles between the time steps. The largest rates of bedrock elevation change correspond to the locations and time periods when the knickpoint is migrating upstream.

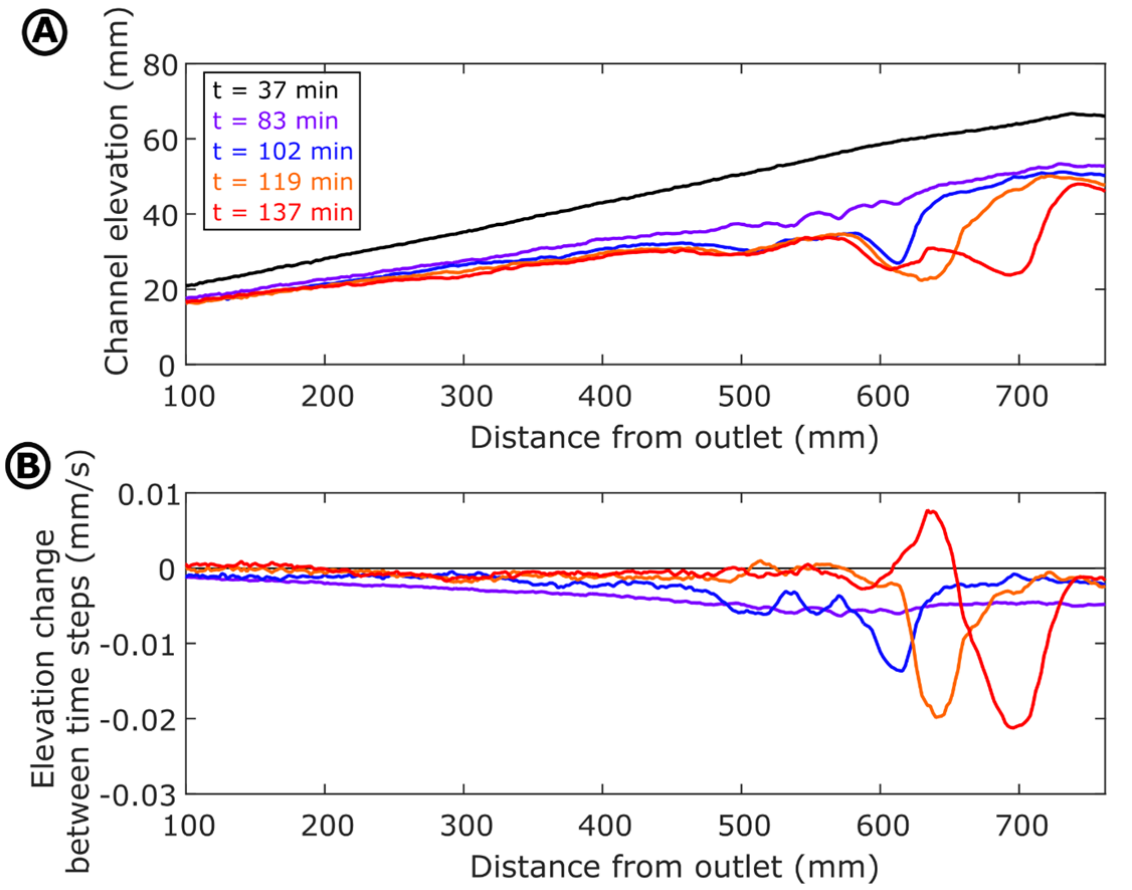

Fig. DR7: (A) Selected long profiles showing alluvial channel just before sediment supply stopped (t = 37 min; black), channel containing cyclic steps, after sediment has been stripped away from the bedrock profile (t = 83 min; purple) and then three long profiles from different stages of knickpoint retreat (t = 102, 119, 137 min; blue, orange and red, respectively). (B) The variation in rate of elevation change with distance along the channel between the different time steps. The consistently high rate of elevation change from t = 37 minutes to t = 83 minutes (purple line) corresponds to the time period when the alluvial cover was being stripped downstream.

Section 5:

Conditions for cyclic step and knickpoint development

'Supercritical knickpoints' were generated during the experiments in the absence of any base level fall, after the development of instabilities in the channel bed possibly associated with supercritical flow conditions, when the Froude number ($Fr = U/(gH)^{0.5}$), is > 1 (Fig. DR9; Parker and Izumi, 2000). In this section, we used the Floodos hydrodynamic model output to calculate the Froude number for all locations within the channel (Fig. DR8) for selected times of experiment 1 (t = 81 min, when bed instabilities were developing; Fig. DR8A, and t = 106 min, when a single knickpoint had formed; Fig. DR8B).

Cyclic steps form under supercritical flow conditions due to an interaction between the channel bed and the flow above it (Izumi et al., 2017), developing a series of steps with transcritical flow that alternates between supercritical and subcritical flow with hydraulic jumps (Fig. DR8A). After a single

knickpoint formed, a pronounced change in the Froude number and a hydraulic jump is present at the knickpoint lip, with subcritical flow conditions present in the plunge pool downstream (Fig. DR8B). The absolute values of Fr are possibly slightly overestimated due to the use of the laminar flow option in *Floodos,* and some uncertainty related to whether the flow is purely laminar or transitional (Fig. DR2). However, the pattern of Fr variation is consistent with cyclic step development as observed and predicted theoretically under supercritical flow conditions (Parker and Izumi, 2000; Izumi et al., 2017).

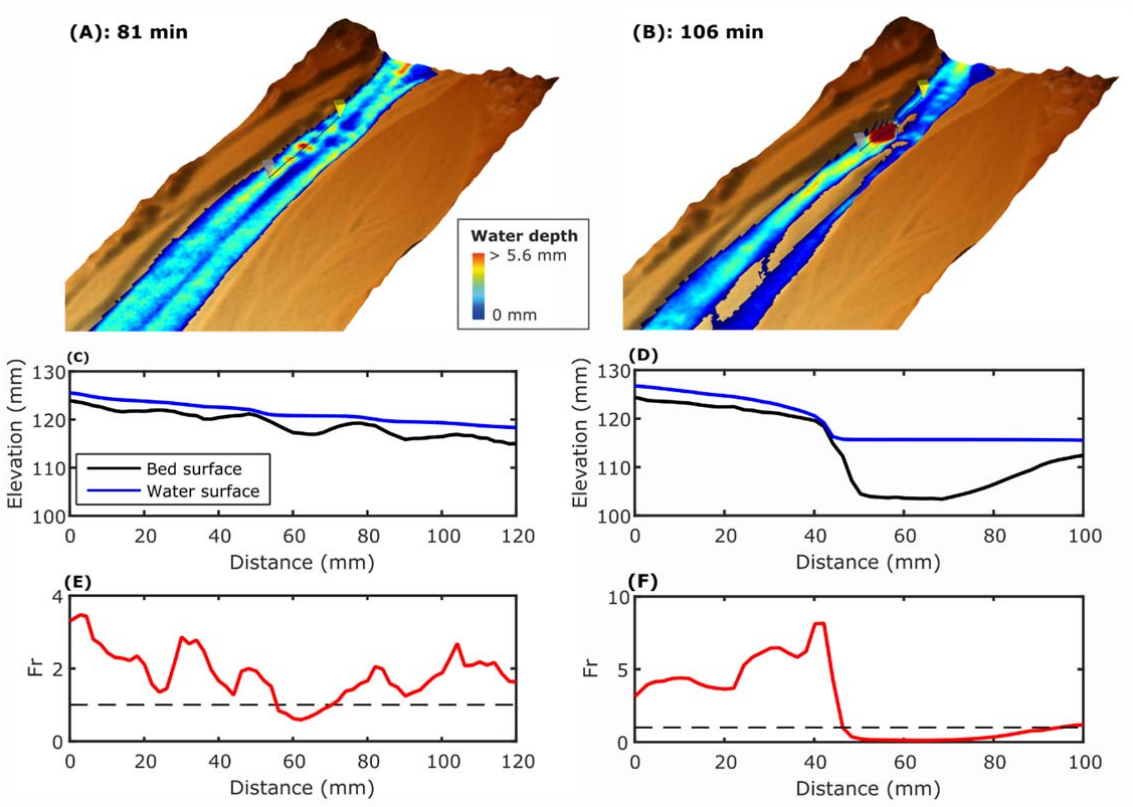

Fig. DR8: Exploration of flow conditions during the development of the self-formed knickpoints. **(A-B)** Topography during the experiments at selected time steps, with the colours indicating the water depth. **(C-D)** Profiles for the bed and water surfaces for the reach along the black lines in (A) and (B). **(E-F)** Extracted Froude number along the same reach as the (C) and (D).

Supercritical flow in natural rivers

Here, we performed a simple test to consider whether supercritical flow conditions can be sustained in natural rivers under steady, uniform flow, by exploring the impact of varying channel width and discharge on the Froude number, assuming a rectangular channel with a constant slope.

The flow velocity can be estimated using the Manning's equation ($U = n^{-1}.H^{2/3}.S^{0.5}$), where n is the Manning's roughness coefficient, H is the flow depth, and S is the channel slope. The flow velocity is also given by U = Q / WH, where Q is the discharge and W is the channel width. Substituting these two equations into each other gives the following equation for the flow depth:

$$H = \left(n \frac{Q}{W}\right)^{\frac{3}{5}} S^{-\frac{3}{10}} \qquad \text{(S2)}$$

The Froude number is calculated from the flow velocity, the acceleration due to gravity (g) and the flow depth: ($Fr = U/(gH)^{0.5}$). Substituting equation S2 into this equation gives the following relationship between the Froude number and the discharge, slope, width and Manning's roughness coefficient:

$$Fr = Q^{\frac{1}{10}} S^{\frac{9}{20}} W^{-\frac{1}{10}} n^{-\frac{9}{10}} g^{-\frac{1}{2}} \qquad \text{(S3)}$$

Eq (S3) shows that in steady uniform flow conditions, the Froude number is mostly sensitive to slope and roughness, with a weak dependency on width and discharge.

According to Parker et al., (2007), the channel width and channel slope of a gravel bed river at bankfull discharge conditions can be calculated using the following equations:

$$W_{bf} = \frac{4.63}{g^{\frac{1}{5}}} Q_{bf}{}^{0.4} \left(\frac{Q_{bf}}{\sqrt{g D_{50}} D_{50}{}^2} \right)^{0.0667} \qquad \text{(S4)}$$

$$S_{bf} = 0.101 \left(\frac{Q_{bf}}{\sqrt{g D_{50}} D_{50}{}^2} \right)^{-0.344} \qquad \text{(S5)}$$

Where Q_{bf} is the bankfull discharge, W_{bf} is the channel width at bankfull conditions, S_{bf} is the channel slope at bankfull conditions and D_{50} is the median grain size. Using these relationships, we calculated the Froude number for bankfull conditions at a range of discharges in an idealized gravel bed river, assuming a median grain size of 10 cm and two values of the Manning's roughness coefficient. The Froude number at equilibrium conditions using the relationships proposed by Parker et al., (2007) are subcritical, typically in the range 0.2-0.3, whatever the value of the bankfull discharge. This shows that in steady uniform flow conditions, single thread gravel bed rivers are not expected to be close to supercriticality, and would not do so even after significant narrowing due to the weak dependency of Fr on channel width (eq. S3). The Parker et al., (2007) relationships (equations S4, S5) are empirical based on a dataset of 72 gravel bed rivers in the UK, Canada, and the USA, which exhibit a degree of universality between them, but do not pertain to braided rivers which are very often the state of rivers during terrace aggradation phases (e.g., Hanson et al., 2006). Using high resolution lidar topography and the *Floodos* hydrodynamic model, we explored the characteristics of the flow conditions at bankfull conditions for a braided river, the Rakaia river in New Zealand. The present day conditions of the Rakaia are a good analogue both for the initial conditions of the experiments and for the former conditions of many present day rivers that are incised with flights of terraces abandoned on the valley sides (e.g., Charwell River, New Zealand; Bull, 1990).

The supercritical flow conditions that initiated the development of cyclic steps in the experiments (Fig. DR9) occurred after channels had narrowed following the initial stripping of the sediment cover. Therefore, we performed some simple tests using the DEM of the Rakaia river to explore the impact of different constant channel widths with a fixed discharge on the Froude number (Fig. DR9A), and the impact of different discharges in a constrained fixed width channel (Fig. DR9B). For a fixed discharge, a narrower channel increases the average value of the Froude number and for a fixed width, increased discharge also increases the average values of the Froude number.

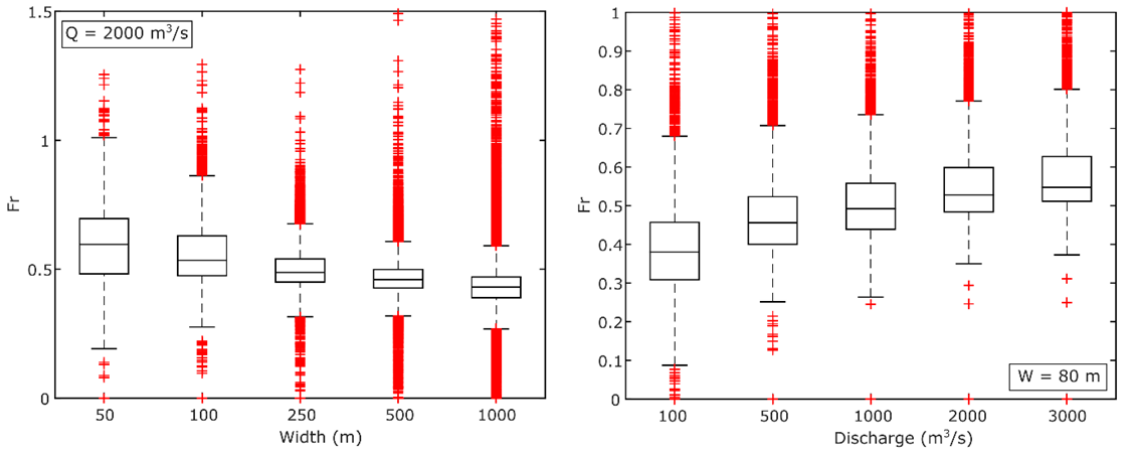

Fig. DR9: (A) Impact of channel width on Froude number for a fixed discharge (Q = 2000 m^3 s^{-1}). (B) Impact of discharge on Froude number for a fixed width (W = 80 m). As predicted by equation S3, both width and discharge have a small impact on the average Froude number in the channel, but the flow can become supercritical in a few locations.

The average values of the Froude number remain sub-critical for the scenarios presented in Fig. DR9, but the peak values of Fr approach supercriticality due to the local spatial variations in the flow conditions. The numerical simulations in Fig. DR11 were carried out using a straight channel, which is overly simplistic for a natural river system. The maps of Froude number for the Rakaia (Fig. DR10B) river indicate that flow conditions are not spatially uniform at bankfull discharge and are subcritical (Fr < 1) but the values of the Froude number can be higher (~0.4-0.6) than the values predicted by the relationships of Parker et al., (2007). However, it is possible to have supercritical flow conditions during frequent floods when the flow is focussed into a narrower channel with a spatially non-uniform channel width (Fig. DR10C-E). Such conditions may be present in natural settings following a perturbation to the sediment supply or transport capacity and the subsequent stripping of sediment cover and focussing of the flow into a significantly narrower channel with spatially variable width (Fig. 2A). The simulations in Fig. DR10 were carried out with no alteration to the channel slope. If the slope of the bedrock surface is steeper than the slope of the alluvial channel flowing over the sedimentary deposits (e.g. Finnegan and Balco, 2013), the likelihood of supercritical flow and the possible development of bed instabilities that evolve into knickpoints is increased. We therefore suggest that the processes leading to rapid strath terrace generation through self-formed knickpoint retreat, in the absence of any vertical perturbation to the bed elevation, identified in the experiments are possible in natural environments.

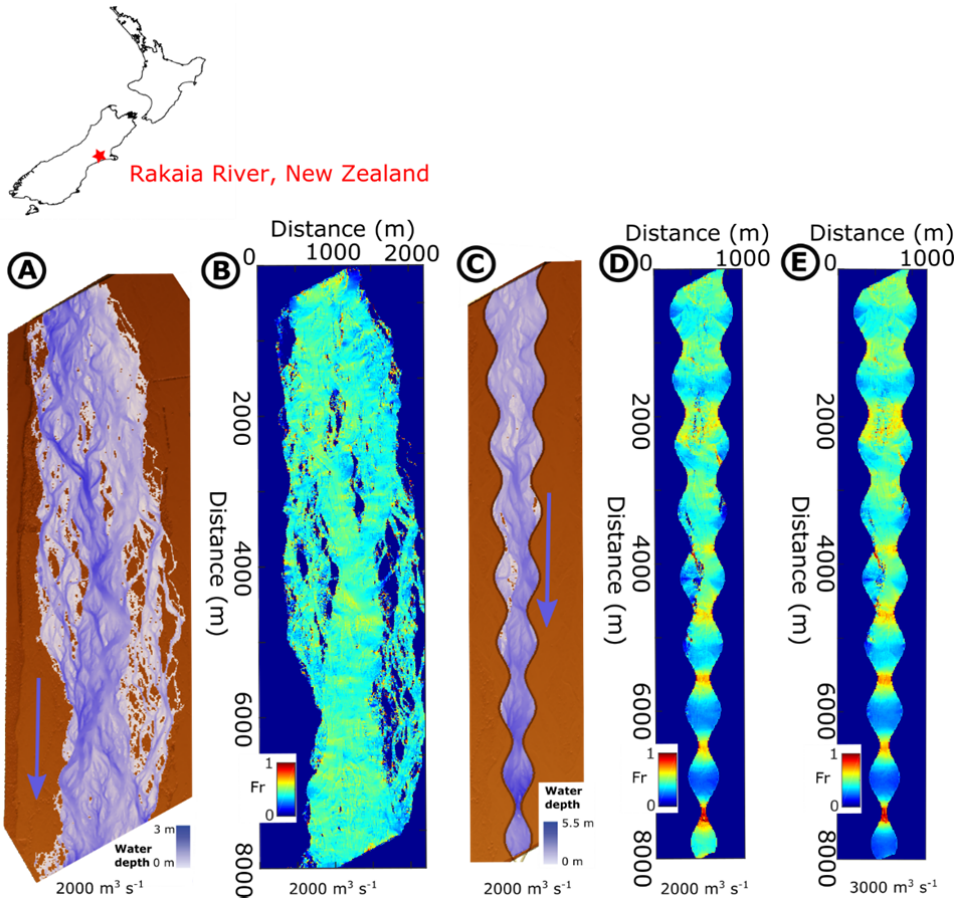

Fig. DR10. **(A)** Map of water depth for a reach of the Rakaia river, New Zealand, under bankfull conditions (Q = 2000 m^3 s^{-1}), modelled using *Floodos* on a Lidar generated DEM (Released under Creative Commons By Creative Commons Attribution 3.0 New Zealand Link: http://data.linz.govt.nz/license/attribution-3-0-new-zealand/; downloaded from www.opentopography.org; DOI: 10.5069/G9JQ0XZV). **(B)** Map of Froude number, typically ~0.4, with some local areas slightly higher at ~0.6. Channel width variability and degree of channel constriction has impact on the water depth **(C)** and Froude number at Q = 2000 m^3 s^{-1} **(D)** and Q = 3000 m^3 s^{-1} **(E)**, with increasing degree of supercriticality with increased channel constriction and increased discharge.

References

Baynes E.R.C., Lague D., Attal M., Gangloff A., Kirstein L.A., Dugmore A.J., 2018, River self-organisation inhibits discharge control on waterfall migration: Scientific Reports 8, 2444, https://doi:10.1038/s41598-018-20767-6

Davy P, Croissant T, Lague D (2017) A precipiton method to calculate river hydrodynamics, with applications to flood prediction, landscape evolution models and braiding instabilities. Journal of Geophysical Research. Earth Surface, v. 122, p. 1491–1512, https://doi.org/10.1002/2016JF004156

Finnegan N.J., Roe G., Montgomery D.R., Hallet B., 2005, Controls on the channel width of rivers: Implications for modelling fluvial incision of bedrock: Geology, v. 33 (3), p. 229-232

Hanson PR, Mason JA, Goble RJ (2006) Fluvial terrace formation along Wyoming's Laramie Range as a response to increased late Pleistocene flood magnitudes. Geomorphology 76, 12-25

Hooke, R. 1968, Model Geology: Prototype and Laboratory Streams: Discussion: Geological Society of America Bulletin, v. 79, p. 391–94, https://doi.org/10.1130/0016-7606(1968)79[391:MGPALS]2.0.CO;2

Izumi N, Yokokawa M, Parker G (2017) Incisional cyclic steps of permanent form in mixed bedrock-alluvial rivers. Journal of Geophysical Research. Earth Surface, v. 122, p. 130–152, https://doi.org/10.1002/2016JF003847.

Paola, C, K M Straub, D C Mohrig, and L Reinhardt. 2009. "The ``unreasonable Effectiveness'' of Stratigraphic and Geomorphic Experiments." Earth-Science Reviews v. 97, p. 1–43.

Parker G, Izumi N (2000) Purely erosional cyclic and solitary steps created by flow over a cohesive bed. Journal of Fluid Mechanics, v. 419, p. 203–238, https://doi.org/10.1017/S0022112000001403.

Parker G, Wilcock PR, Paola C, Dietrich WE, Pitlick J (2007) Physical basis for quasi-universal relations describing bankfull hydraulic geometry of single-thread gravel bed rivers. Journal of Geophysical Research, v. 112, F04005.